

PAPER • OPEN ACCESS

Coherent, high repetition rate tender x-ray free-electron laser seeded by an extreme ultra-violet free-electron laser oscillator

To cite this article: V Petrillo *et al* 2020 *New J. Phys.* **22** 073058

View the [article online](#) for updates and enhancements.



PAPER

Coherent, high repetition rate tender x-ray free-electron laser seeded by an extreme ultra-violet free-electron laser oscillator


OPEN ACCESS

RECEIVED
2 January 2020REVISED
18 May 2020ACCEPTED FOR PUBLICATION
11 June 2020PUBLISHED
29 July 2020

Original content from
this work may be used
under the terms of the
[Creative Commons
Attribution 4.0 licence](#).

Any further distribution
of this work must
maintain attribution to
the author(s) and the
title of the work, journal
citation and DOI.



V Petrillo^{1,2,3,7}, M Opromolla^{1,2,3}, A Bacci^{2,3}, F Broggi^{2,3}, I Drebot^{2,3}, G Ghiringelli⁴ ,
E Puppin⁴, M Rossetti Conti^{2,3}, A R Rossi^{2,3}, M Ruijter^{2,3,5}, S Samsam^{2,3,5,6},
A Tagliaferri⁴, G Rossi¹ and L Serafini^{2,3}

¹ Università degli Studi di Milano, Via Celoria 16, 20133 Milano, Italy

² INFN-Sezione di Milano, Via Celoria 16, 20133 Milano, Italy

³ LASA, Via F. Cervi 201, 20090 Segrate (MI), Italy

⁴ Politecnico di Milano, P.zza Leonardo da Vinci, 20133 Milano, Italy

⁵ Università 'La Sapienza', Piazzale Aldo Moro, 5, 00185 Roma, Italy

⁶ University of Mohamed V, Rabat, Morocco

⁷ Author to whom any correspondence should be addressed.

E-mail: vittoria.petrillo@mi.infn.it

Keywords: free electron laser, oscillator, superconducting linac

Abstract

A seeded FEL driven by a linac based on superconducting cavities, generating 10^8 – 10^{10} coherent photons per shot at 2–5 keV with 0.2–1 MHz of repetition rate, can address the need of a source devoted to fine analysis of matter using the linear spectroscopy technique. The seeding scheme described hereafter is a multi-stage cascade upshifting the radiation frequency by a factor 20–40. The x-ray range can be achieved with a seed constituted by a coherent flash in the extreme ultraviolet range provided by an FEL oscillator operating at 12–14 nm. The whole chain of x-ray generation is described by means of start-to-end three-dimensional simulations.

1. Introduction

The generation of free-electron laser (FEL) radiation with high longitudinal coherence degree in the x-ray range is a very demanding and stimulating research field aimed at producing a tool for the fine time-resolved analysis of matter, with applications extending from the life sciences to material physics. The most common operational mode of x-ray FELs is the self amplified spontaneous emission (SASE), where the amplification starts from the electron shot noise and its longitudinal coherence is intrinsically limited by the stochastic nature of the start-up process. Partial longitudinal coherence can be achieved by using very short electron bunches to produce single spiked SASE radiation [1–3] or by means of self-seeding processes [4, 5], though with very low pulse-to-pulse stability. The seeded amplifier configuration, where the radiation starting phase is forced by an external narrow-bandwidth coherent source well above the electrons' shot noise power, instead, allows to attain the highest degree of temporal coherence and pulse stability within a shorter distance. FERMI@Elettra [6, 7] represents the unique example of FEL amplifier of a laser seed pulse in operation, with negligible time jitters and minor pulse to pulse intensity fluctuations. It operates down to wavelengths of 4 nm with a repetition rate up to 50 Hz. Ti:Sa laser pulses and its harmonics are particularly suitable as seed for their characteristics in terms of energy (J-class), pulse shortness (fs-class) and stability. However, these lasers do not provide intense radiation below 120 nm of wavelength, thus impeding the direct seeding [8] in the soft–hard x-ray range, where other seeding schemes should be foreseen. As demonstrated at FERMI down to the soft x-ray domain [9], high gain harmonic generation (HG) in multistage cascades allows to produce short wavelength radiation with energy level comparable to the SASE mode, but with full temporal coherence and small energy fluctuations [10, 11]. In this configuration, external laser pulses seed the electron beam in a first undulator segment, the modulator, inducing it to emit the laser frequency itself and its harmonics. A further undulator segment, the radiator, tuned at the n th harmonics of the previous stage radiation, forces the electron beam to emit coherently this

resonant frequency. The seed encodes its coherence degree on the FEL radiation, determining the temporal and spectral distribution of the output. Seeded FEL amplifier operation, in combination with the generation of harmonics of an IR laser in crystals, has been shown experimentally in the optical-UV range [10, 12], demonstrated and routinely performed at FERMI up to few nm of wavelength [9]. The reliability of this scheme in the hard x-ray spectral range, however, has still to be proven. Besides the harmonics' generation in crystals, the radiation obtained with high harmonic generation (HHG) processes in gases [13, 14] could also be used as seed for FELs [15–17]. Though inherently inefficient, the harmonic radiation produced in gases could be sufficient to overcome the electron shot noise level down to 12–20 nm, permitting to reach the x-ray domain by means of cascades. The echo-enhanced harmonic generation (EEHG) technique [18–21] efficiently reaches the range between extreme ultra-violet and soft x-ray frequencies and presents good perspectives also toward the hard x-rays. However, despite the recent strong development in the laser community, operations at high repetition rate are up to now difficultly implementable for all the seeding schemes based on conventional lasers.

FEL oscillators [22–24] in the soft/hard x-ray range (XFEL) [25] and regenerative amplifiers (RAFEL) [26–28] have been proposed as direct source of monochromatized coherent x-rays [25, 29, 30] or as source of seed for subsequent cascades [31]. In this paper, we show a method for producing high-repetition rate, truly coherent and stable tender x-ray pulses, based on a multi-stage cascade seeded by an extreme ultra-violet (VUV) FEL oscillator driven by electron beams at the same energy of those alimending the FEL cascade. The electron beam is supposed to be accelerated with the two-pass two-way scheme in the compact super-conducting accelerator equipped with an arc compressor [33], proposed for the MariX project (multi-disciplinary advanced research infrastructure for the generation and application of x-rays) [32]. MariX should provide 1 MHz, 2–3.8 GeV electron beams with 0.3 mm mrad of emittance at few 10^{-4} of energy spread. The use of the superconducting techniques guarantees particularly high electron beam stability [34–36]. Low temporal shot to shot jitters, joint to seeding schemes, allow to reach a high level of radiation stability [37]. The oscillator driven by 2–2.6 GeV electron bunches radiates about 13 nm of wavelength, a value where efficient multilayer mirrors exist and have been widely tested. The oscillator seed is then injected into a triple cascade with an up-shift frequency factor of 20–40, thus reaching a few Ångström-class radiation. The seeded high repetition rate FEL source MariX is tailored for time-resolved spectroscopy with coherent x-rays: therefore, the energy of the individual pulses, at wavelengths of about 6–2 Å, should not exceed the linear response threshold [38]. This implies 10^7 – 10^{10} photons at the FEL exit per 10 fs-long pulses at several hundred kHz of repetition rate. High longitudinal coherence will enable pump–probe methods at 10–100 fs accuracy and with high statistics. This option will actually benefit precision timing measurements as the SASE intrinsic pulse-to-pulse jitters will be substantially eliminated, as well as the reduced pulse-to-pulse intensity fluctuations, thus approaching the unique performance of FERMI@Elettra [7] at x-ray energies.

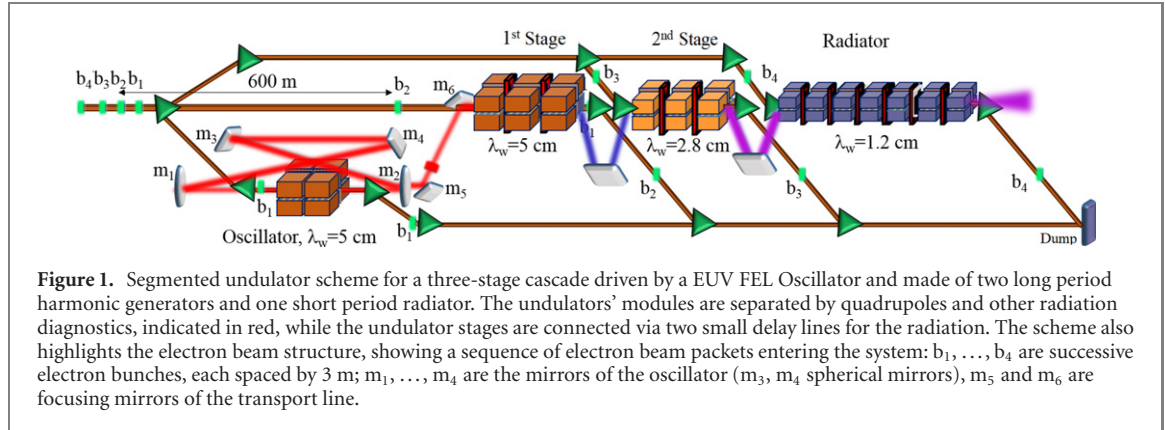
The paper is organized in the following way: the FEL layout is described in section 2. In section 3.1, the seeded source is analyzed: the behavior of the oscillator, as well as the subsequent 5×5 and 7×5 cascades in section 3.2, is described by means of full three-dimensional and time-dependent simulations. We discuss the nominal parameters of this scheme with realistic parameters comparing them with the SASE output. Final comments on the implementation of this scheme will be presented in the conclusions.

2. FEL accelerator layout

All our analyzes rely on the electron beam foreseen by the accelerator of the MariX project presented in reference [32]. MariX is based on the innovative design of a two-pass two-way superconducting linear electron accelerator, equipped with an arc compressor [39, 40], to be operated in CW mode at 1 MHz. Its layout is discussed in details in reference [33]. The injector is capable of producing trains of four electron bunches, with a repetition rate of 0.5 MHz and a spacing of 10 ns between electron bunches and 2 μ s between different trains. The characteristics of the electron beam, as evaluated after start-to-end simulations from the cathode, through the sequence linac-arc-linac, to the exit of the accelerator, are listed in table 1. The electron beam longitudinal phase space distribution was manipulated by adding two additional quadrupoles and steering magnets in the arc and by introducing a dedicated dogleg upstream the FEL to remove the residual dispersion, resulting in the distribution shown in figure 12 of reference [33]. As studied and demonstrated in reference [34], the superconducting technology allows to achieve low jitters and fluctuations of the electron beam. These increased stability conditions, together with the seeded mode FEL operation, give the possibility to produce a fully coherent, high repetition rate and highly stable x-ray source.

Table 1. Electron beam for MariX FEL.

Electron beam energy	GeV	1.6–3.8	Rms relative energy spread	10^{-4}	5–3
Charge	pC	8–50	Electron bunch duration	fs	2.5–16
Current	kA	1.3–1.6	Slice energy spread	10^{-4}	4–2
Rms normalized emittance	mm mrad	0.3–0.5	Slice normalized emittance	mm mrad	0.3–0.5



After the second passage through the linac, the electron beam is matched to the undulator device. To obtain radiation with wavelength in the desired range (6–2 Å, or in energy 2–5 keV) with the moderate electron energy provided by the MariX superconducting accelerator (at maximum 3.8 GeV), a radiator constituted by a short period undulator is considered. According to the resonance condition

$$\lambda = \frac{\lambda_w}{2\gamma^2}(1 + a_w^2), \quad (1)$$

where a_w is the undulator parameter and γ the electron Lorentz factor, we can deduce that a period of $\lambda_w = 1.2$ cm is suitable to cover the desired wavelength range. The global structure of the undulator, instead, depends on the seeding scheme and emission mechanism.

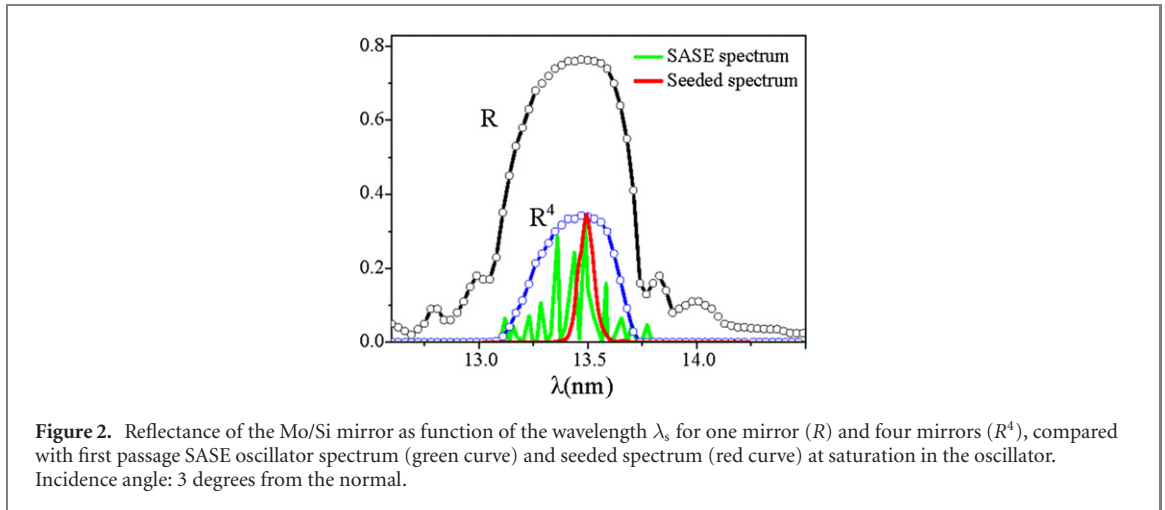
3. Seeded FEL operation

The cascaded seeded FEL considered for MariX is based on the segmented undulator scheme shown in figure 1, consisting of two stages of longer period undulators (respectively of period $\lambda_w = 5$ cm and 2.8 cm) for the harmonic generation process and a third shorter period ($\lambda_w = 1.2$ cm) undulator as radiator.

3.1. The seeding source

The seed is delivered by an oscillator working at $\lambda_0 = 13.6$ nm, schematically represented on the left of figure 1. Each electron bunch train is made of four electron bunches spaced by 10 ns and only the front electron bunch (b_1 in figure), at the head of each train, seeds the oscillator. Since the electron beam alighting the system is deteriorated by the radiation process, it is dumped after the passage into the oscillator undulator, and the radiation inside the oscillator is synchronized with the following head electron bunch. The repetition rate of the FEL radiation yield turns out to be 0.5 MHz. Due to the rather low electron bunch length and the need to preserve its quality throughout the whole FEL line, the other three electron bunches of each train (b_2, b_3, b_4 in figure) are delivered, through three dedicated transfer lines, to the entrance of each cascade stage. This scheme requires a high repetition rate electron beam, an undulator to provide FEL gain and an optical cavity to recirculate the radiation, allowing it to interact with following fresh electron bunches over many passes.

The oscillator, alighted by the electron beam at about 2.0 GeV, is constituted by an undulator segment with period $\lambda_w = 5$ cm and $a_w = 2.77$, similar to the first undulator of the cascade. It is embedded into a folded ring cavity composed by a minimum of 4 mirrors, two of which focusing. For an oscillator repetition rate of 0.5 MHz, the total cavity length L_c should be 600 m and, considering for instance 4 mirrors, the distance between two of them is about $L_c/4 = 150$ m. Besides the specifics of the electron beam, the oscillator output depends on the length of the undulator module, on the reflectivity and length of the optical round trip line, given by the recirculation distance L_c minus the slippage length $N_w\lambda_0$ accumulated in the undulator (N_w being the number of undulator periods). The full calculation of the oscillator



supermodes [26] is here performed completely numerically in a way similar to that described in reference [23]: extracting the radiation field simulated by GENESIS 1.3 from the oscillator undulator, driving it through the optical line accounting for the effects of mirrors and propagation, and superimposing it on the successive electron bunch. The microscopic distribution of the electron beam is changed shot to shot.

3.1.1. The mirrors

The oscillator wavelength, $\lambda_0 = 13.6$ nm, corresponds to the optimum wavelength for Mo/Si multilayer mirrors [41, 42]. The effect of the mirror on the radiation pulse is described by the transformation:

$$E(\underline{x}') = \int d\underline{k} R(\underline{k}) \int d\underline{x} E(\underline{x}) e^{i\underline{k} \cdot (\underline{x} - \underline{x}')} \quad (2)$$

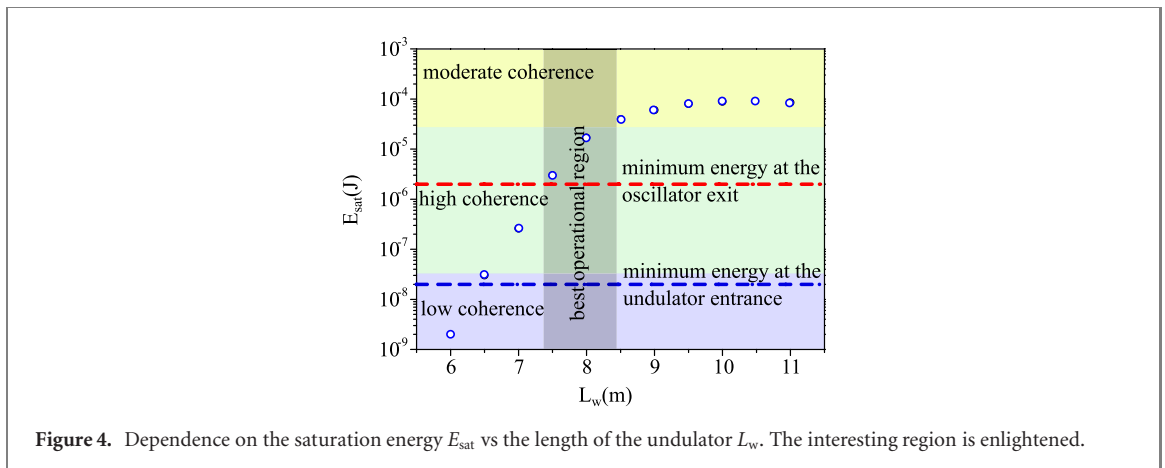
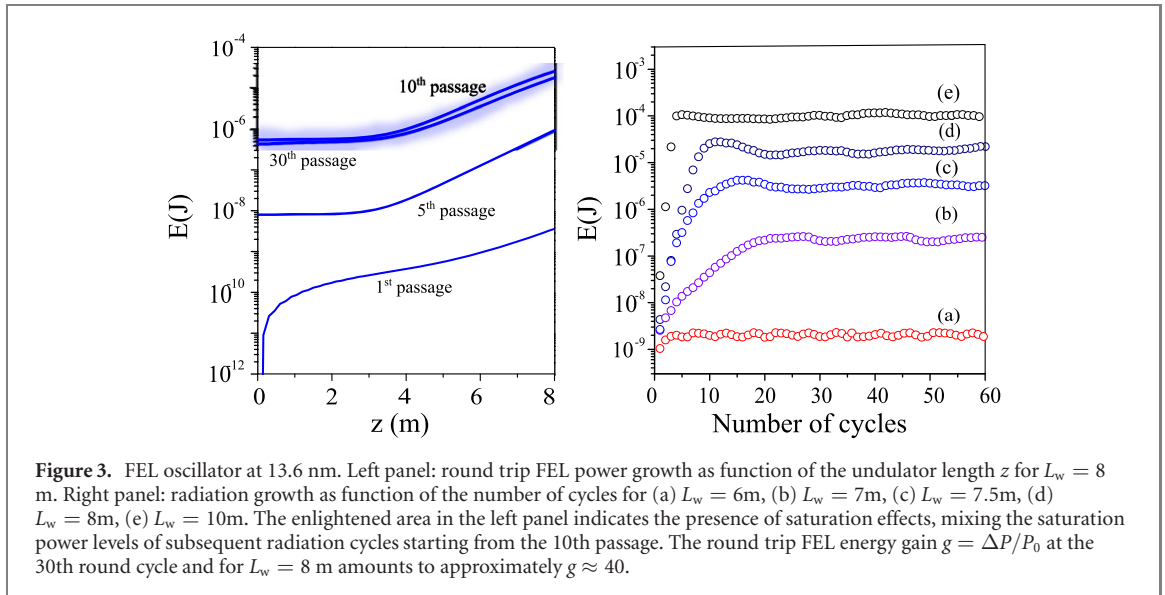
where E is the electric field, R is the mirror reflectance and $\underline{k} = 2\pi/\lambda_0$ is the radiation wave vector. As shown in figure 2, the reflectivity of one mirror in normal or quasi-normal incidence exceeds $R = 0.75$, with the optical line's transfer function width of the same order as the SASE bandwidth and much larger than the seeded radiation spectra [42].

The spectral filtering of the mirrors is therefore important in the first stage of the cavity loading only, and then almost completely inessential. The angular filtering is also ineffective, because the mirror acceptance is about 0.15 rad [43], a value extremely larger than the divergence of the FEL pulse, of the order of hundreds–tens μ rad. The purification of spectral and temporal distributions occurs via the reiterated amplification of the best SASE spike. The reflectivity after four reflections is about $R^4 = 0.3$, while the fraction coupled to the line matching the seed to the first cascade module consists of about 25% of the oscillator yield.

3.1.2. The undulator

The operation of the oscillator is shown in figure 3: the left panel reports the round trip power growth versus the undulator length for $L_w = 8$ m in few significant cases, while the right panel shows the energy loading as function of the number of round cycles for different values of the undulator length L_w from 6 to 10 m. This range corresponds to the best FEL operation, that should be at about $L_w = 2\pi Z_R$ (Z_R being the Rayleigh length). For an electron beam with $\sigma_{x,y} \approx 35 \mu\text{m}$ the Rayleigh length is about 1.1–1.2 m, and L_w turns out to be indeed of the order of 7.5 m. The oscillator goes to saturation in about 10–50 passages, depending on L_w , with slight intensity oscillations around the final average value E_{sat} , a sort of breathing of the system already observed in reference [44]. As reported in the left panel for the case $L_w = 8$ m, the same occurs to the round trip power growth, which oscillates after the 10th radiation passage in the cavity.

In the case of shorter undulators ($L_w < 7$ m), the radiation saturates at a very low level ($E \sim 1$ nJ) and the coherence stage is not reached. Intermediate states with $7 \text{ m} < L_w < 9$ m show moderate energy values ($E \sim 100$ nJ to $10 \mu\text{J}$) but high coherence levels, attained in 30–50 cycles. For undulators larger than 9 m, tens–hundreds μJ are emitted with moderately good longitudinal coherence in about ten cycles. Non linear saturation effects appear in the case of longer undulators ($L_w \gtrsim 9$ m), with the effect of deteriorating the coherence degree. The dependence of the saturation energy with respect to the undulator length, presented in figure 4, shows a threshold for the emission at around 7 m. The different microscopy presented by the



successive electron bunches flowing in the oscillator superimposes a general irregularity to the natural oscillations; slight indentations, more evident for shorter undulators, delay the saturation.

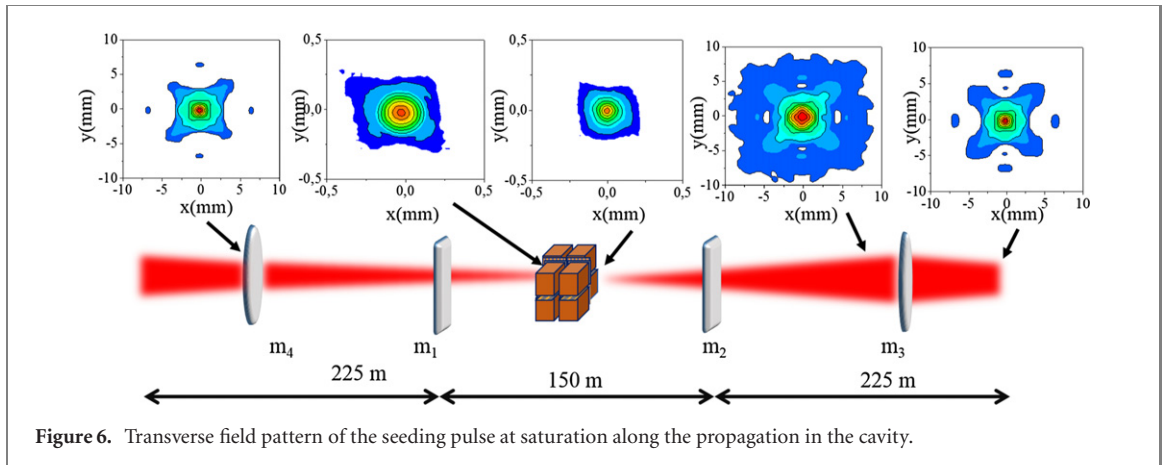
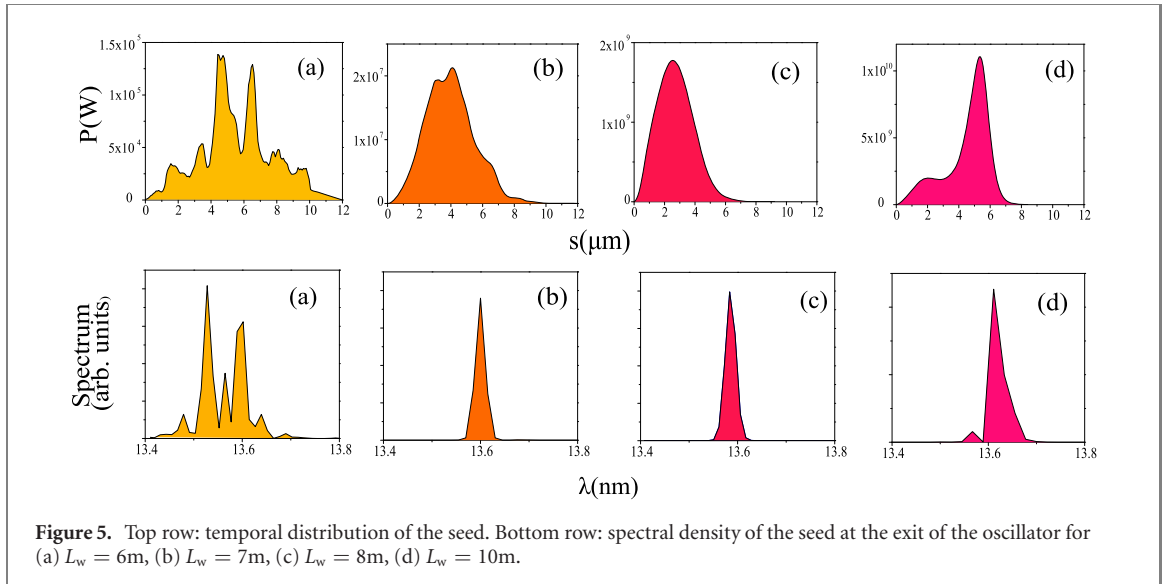
Figure 5 reports the pulse temporal and spectral densities at saturation in various cases. The choice of the undulator length has been done by searching the optimum value of the seed intensity at the first cascade stage, with the aim of producing harmonics of high quality in the first stage of the cascaded FEL. On one side, the seed must overcome the undulator spontaneous emission. On the other side, a too intense seed produces very strong non linear effects in the electron beam with non-controllable and not single spiked harmonics' production. Therefore the seed energy should be between few tens and hundreds nJ at the entrance of the cascade (i.e. 20–100 nJ). The mirrors are supposed to be micrometrically movable and turnable in order to compensate the shift between the radiation and the electrons introduced by the slippage, of the order of 1 μm , stabilizing the output.

3.1.3. The cavity

The cavity is composed by two plane and two spherical mirrors with curvature radius \mathcal{R} , disposed as shown in figure 6 and all interspersed by drifts. The optical line is described by a round trip 2×2 matrix with elements depending on the distance between mirrors and on their focal lengths. The field after the transport is given by the modified Huygens' integral [48]:

$$E(\underline{x}') = \int dx dy \frac{iE(\underline{x})}{B\lambda_0} e^{-\frac{i\pi}{\lambda B}(A(x^2+y^2) - 2(xx' + yy') + D(x'^2 + y'^2))}$$

with the round trip matrix elements A , B , C and D . Stable operation of the cavity needs a focal length $f = \mathcal{R}/2 > L_c/4$. The distance between the second focusing mirror and the undulator entrance is about 225 m (see figure 6) and, in order to have the maximum focusing of the radiation around the undulator center, in our case we chose $f = 225.7$ m. Figure 6 shows the transverse pattern of the electric field of the seed at



saturation in few positions along the propagation in the cavity, the undulator being crossed from left to right. It presents a modest component of higher oscillator supermodes, that are partially depleted in the undulator by the FEL itself. The radiation hits the mirrors with a maximum transverse rms dimension $\sigma_{x,y} \approx 1\text{mm}$ and enters the undulators' system with $\sigma_{x,y} \approx 150\text{--}200\ \mu\text{m}$. The FEL amplification process focuses the radiation pulse further, till about $100\ \mu\text{m}$.

3.1.4. The optical transport line

Taking into account the possible EUV power loss due to absorption of the materials, the radiation energy exiting the cavity last mirror is a factor $(1 - R) \approx 0.25$ of the intracavity energy at maximum. Since the seed should meet the successive head electron bunch at the first undulator entrance, it has to be further retarded by $1\ \mu\text{s}$, corresponding to a distance of about $300\ \text{m}$. The radiation transfer line from the oscillator exit to the undulator entrance is constituted by $2n$ mirrors, and its attenuation amounts to $R^{2n} = 0.56^n$ (with $n = 1\text{--}3$). In order to focus the radiation beam further and deplete the remaining high-order modes of the radiation field, the transfer line mirrors might be spherical. The oscillator seed pointing stability and transverse overlap with the electron bunches after the transport line will be checked and adjusted with multipurpose stations and beam stabilization systems as the ones described in references [45–47]. Considering $20\text{--}100\ \text{nJ}$ as the seed energy needed in the FEL, we can evaluate the energy stored in the oscillator as $(20\text{--}100\ \text{nJ}) / [(1 - R)R^{2n}] \sim (80\text{--}400\ \text{nJ}) / 0.56^n$, namely hundreds nJ–tens μJ . These values are indeed obtained with undulator modules of the order or longer than $7.5\ \text{m}$ for the oscillator, confirming the best operational points given by $L_w = 7.5\text{--}9\ \text{m}$. The characteristics of the seed after the last cavity mirror in the most suitable case are summarized in table 2.

Table 2. Characteristics of the seed, generated by the FEL oscillator with undulator length $L_w = 8$ m. The repetition rate of the source is 0.5 MHz. $\$ = \text{photons s}^{-1} \text{mm}^{-2} \text{mrad}^{-2} \text{bw} (\%e)^{-1}$.

λ_0 (nm)	13.6	E (μJ)	20
N/shot	1.3×10^{12}	$N \text{ s}^{-1}$	0.65×10^{18}
bw	1.7×10^{-3}	Duration (fs)	6.6
div (μrad)	50	Size (μm)	80
Peak brilliance ($\$$)	0.7×10^{31}	Average brilliance	2.3×10^{22}

Table 3. Possible operational working points of the cascaded FEL, seeded by the oscillator delivering a wavelength of 13.6 nm.

	λ_w (cm)	1st mod. 5	2nd mod. 2.8	Radiator 1.2
5×3	a_w	2.39	1.18	0.93
$E = 1.8$ GeV	$\lambda(\text{nm})$	13.6	2.72	0.906
7×3	a_w	2.77	1.1	0.85
$E = 2.04$ GeV	$\lambda(\text{nm})$	13.6	1.94	0.647
5×5	a_w	2.77	1.45	0.67
	$\lambda(\text{nm})$	13.6	2.72	0.544
$E = 2.04$ GeV	Length (m)	8	12	10
7×5	a_w	3.31	1.48	0.701
	$\lambda(\text{nm})$	13.6	1.94	0.388
$E = 2.45$ GeV	Length (m)	8	8	12
7×7	a_w	3.61	1.66	0.5
$E = 2.66$ GeV	$\lambda(\text{nm})$	13.6	1.94	0.277

3.2. The cascaded radiation source

Ångström-class radiation can be generated with the cascaded undulators previously shown in the right part of figure 1. The multi-stage cascaded technique uses different undulator stages to generate and amplify the harmonics of the initial seed pulse extracted from the oscillator, obtaining a coherent FEL pulse at higher photon energies.

The three-stage cascade here considered is made of two undulators, operating as harmonic generators, and a third one, the radiator, in which the final harmonics is amplified. In particular the electron beam in a first undulator segment is forced by the oscillator seed to coherently emit the seed frequency itself and its higher harmonics. At the end of this first stage, the n th harmonics is extracted and used as seed for the second stage, tuned at this harmonics. In the second undulator, the m th harmonics of the seed is generated and extracted. The radiator, tuned at the $(n \times m)$ th harmonics of the seed, forces the electron beam to coherently emit this resonant frequency (namely λ_0/nm). The natural focusing power of the undulator and the use of quadrupoles in between the undulators' modules confine the electron envelope. Table 3 reports various resonance options from 9 Å to 2.7 Å.

In order to avoid deteriorating the electron beam and the FEL pulse quality, multi-stage FEL cascades normally make use of the fresh bunch injection technique [49], consisting in superimposing the seed on a portion of the electron beam not affected by the radiation process of the previous stage. However, given the high repetition rate operation and the modest electron bunch duration, we consider three different transport lines delivering the electron bunches (b_2, b_3, b_4 in figure 1) belonging to each electron packet and following the head electron bunch alimentering the oscillator, to the different undulators of the cascade. To synchronize the electron arrival time with the radiation exiting from the different stages, two small delay lines of about 3 m between the first two stages and before the radiator are used. All FEL simulations have been performed with the code GENESIS 1.3 [50].

Here we show the results of the 5×5 and 7×5 cascade, comparing them to the SASE reference case. Considering the electron beam parameters of table 1, with an energy of 2.04 GeV, and an undulator of period $\lambda_w = 1.2$ cm and strength $a_w = 0.67$, the SASE radiation obtained at 5.44 Å, with a charge of 50 pC [case (a)] and 8 pC [case (b)], is shown in figure 7. The coherence of the produced FEL pulses is evaluated by computing the coherence degree, evaluated as

$$\Gamma_{12}(\tau) = \left| \frac{\int dt E_1(t) E_2(t - \tau)}{\sqrt{\int dt |E_1|^2} \sqrt{\int dt |E_2|^2}} \right|, \quad (3)$$

between two different generic pulses (multi-shot case) or for one single pulse (single-shot case, $\Gamma = \Gamma_{1,1}$), and whose range is $0 \leq \Gamma \leq 1$. In expression (3), E_1 and E_2 are the complex electric fields of the pulses as

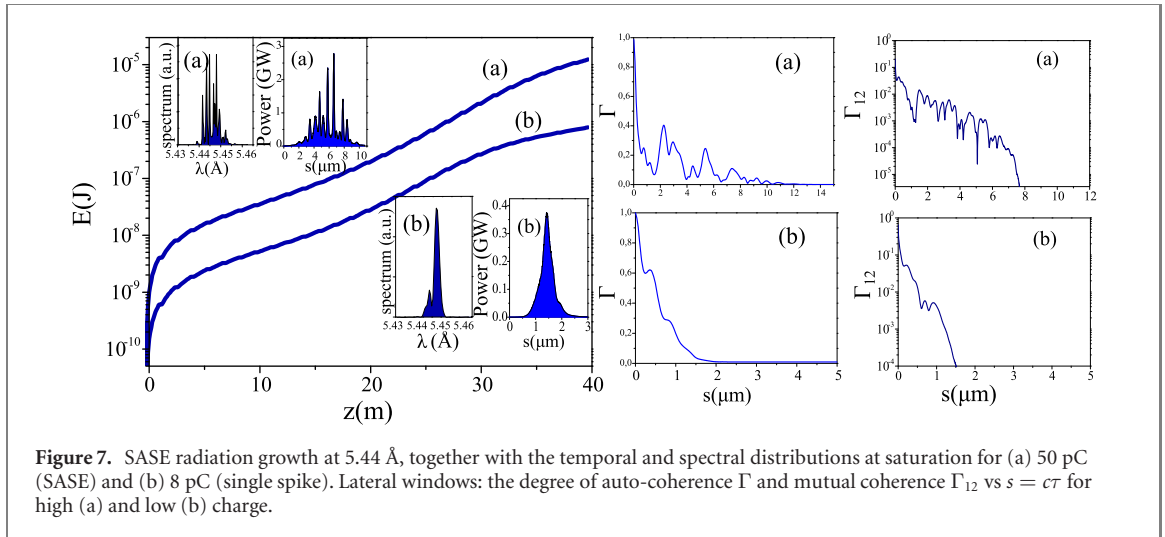


Table 4. MariX FEL characteristics of the analyzed working points. The SASE results are reported at 40 m for the high and low charge case, respectively. The repetition rate of the source is 0.5 MHz. $\$ = \text{photons s}^{-1} \text{mm}^{-2} \text{mrad}^{-2} \text{bw} (\%c)^{-1}$.

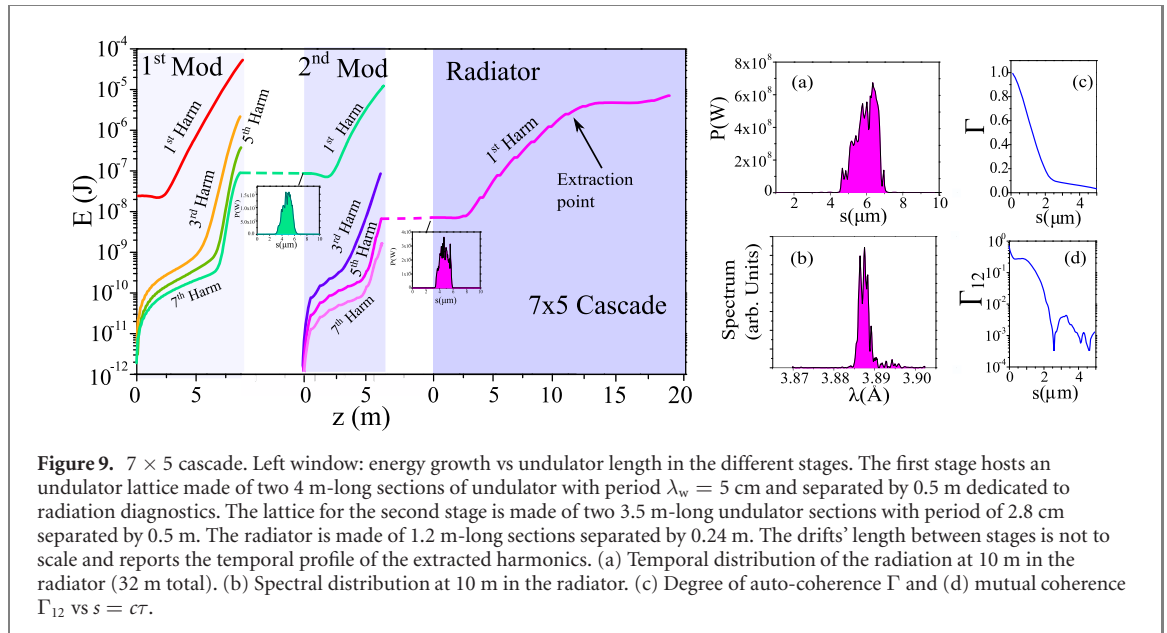
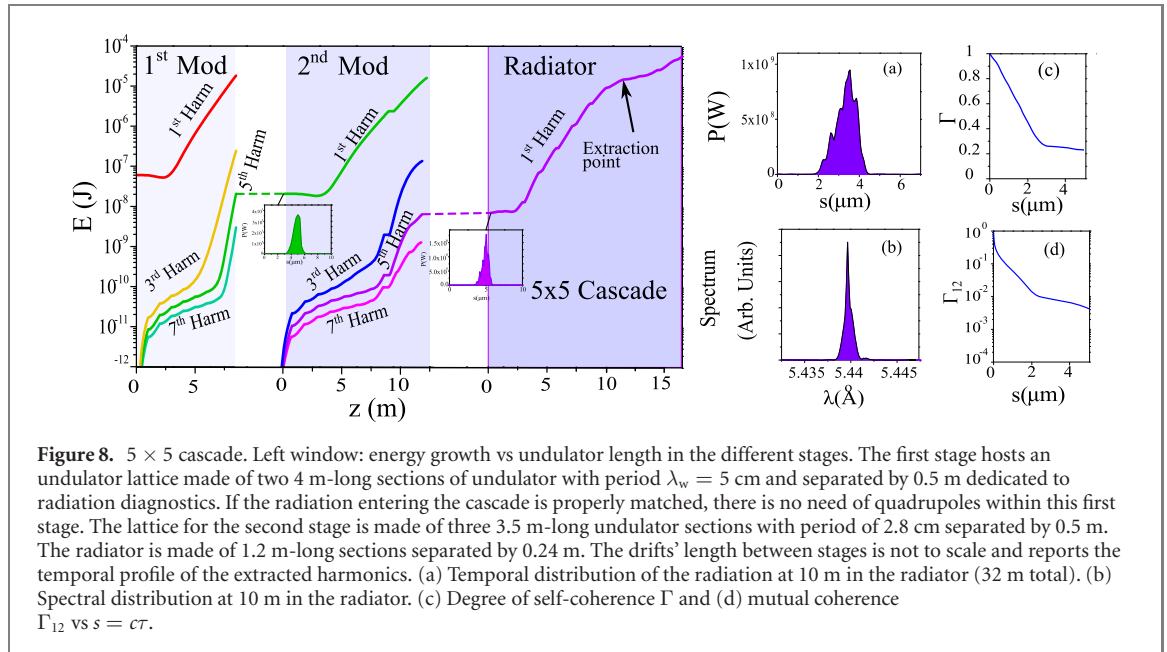
Radiation mode		SASE	5×5	7×5
Electron charge	pC	50–8	50	50
Photon energy	keV	2.27	2.27	3.22
Radiation wavelength	Å	5.44	5.44	3.88
Photon/shot	10^{10}	3.5–0.21	1.9	0.21
Bandwidth	0.1%	5–7.5	0.17	0.32
Pulse length	fs	10–2	3	4.5
Pulse divergence	μrad	39–48	3.6	5
Photon/s	10^{16}	3.5–0.21	0.95	0.11
Average brilliance	$10^{24} \$$	$1.8 \times 10^{-3} - 4.8 \times 10^{-5}$	7.48	0.16
$\Gamma_{12}(0)$		0.1–0.2	1	0.94

function of time. Regarding the SASE emission, this is shown in the lateral windows of figure 7 in both cases of high and low charge electron beams. The SASE radiation characteristics are listed in table 4, third column.

Regarding the cascaded operation, we consider electron beams with a charge of 50 pC and energy specified in table 3. In the case of the 5×5 cascade, the value of the undulator parameter a_w for the first undulator to be resonant at $\lambda = 13.6$ nm is $a_w = 2.77$, fully compatible with its specifics. The second stage operates at $a_w = 1.45$, being resonant with the 5th harmonics of the first module $\lambda = 2.72$ nm. Finally, in order to resonate at the radiation wavelength, 0.54 nm, corresponding to the 5th (25th) harmonics of the second (first) stage, the radiator has $a_w = 0.67$. The energy growth of the fundamental frequency and its first odd harmonics for the cascade performing a 5×5 frequency upshift conversion is presented in figure 8, left window. Saturation occurs in a net total undulator length of 30 m, distributed in 8 m for the first undulator, 12 m for the second and other 10 m in the radiator. The radiation maintains the single spiked temporal and spectral distributions up to the onset of saturation, and then its coherence begins to degrade. The temporal profiles of the harmonics extracted from the different stages is also shown at the end of each drift length in the left window. The temporal and spectral distributions at the extraction point after 10 m in the radiator are presented in figure 8, respectively in window (a) and (b).

The output consists of 2×10^{10} photons per shot in a relative bandwidth of about 1.7×10^{-4} . The coherence factors of one shot Γ and from shot to shot Γ_{12} , in figure 8 window (c) and (d), show the enhanced coherence and stability of the seeded output with respect to SASE and single spike modes. This fact can be appreciated by comparing the graphs in the lateral boxes of figure 7 to those in figure 8: in the cascaded case, the factor Γ experiences a slower decay, and the equal time mutual coherence factor $\Gamma_{12}(0)$ is 1, compared to 10^{-1} in the high charge SASE and to 2×10^{-1} in the single spike case. At the same time, the temporal profile of the radiation are much more stable in the seeded case and do not show the multiple spike's generation of the SASE.

The 7×5 cascade produces radiation at 3.88 Å and needs a more energetic electron beam with energy $E = 2.4$ GeV. The values of the undulator parameters for the 7×5 cascade are reported in table 3. The



energy growth, the radiation profiles after each cascade stage as well as the temporal and spectral distributions and the coherence factors are presented in figures 9(a)–(d). The output of the 7×5 cascade ($\lambda = 3.88 \text{ \AA}$) is 2.1×10^9 photons per shot in a bandwidth of 3.2×10^{-4} . Table 4 summarizes the radiation properties for the high charge and low charge SASE case (third column), the outputs of the 5×5 and 7×5 cascades, respectively presented in the fourth and fifth columns.

4. Conclusions

A new generation accelerator complex is at the core of the MariX facility dedicated and optimized to ultrafast coherent-x-ray spectroscopy and inelastic photon scattering, and to highly penetrating x-ray imaging of mesoscopic and macroscopic samples. Such facility will be intrinsically multi-user and multidisciplinary, as the research performed and science output. In the range of wavelengths between 2 and 6 \AA , MariX provides either 10^{10} – 10^{11} photons per shot with a repetition rate of 1 MHz in SASE mode or 10^9 – 10^{10} photons per shot in the single spike SASE mode. In this paper, we have shown that the radiation from an EUV FEL oscillator can be used as seed for a cascaded FEL, performing a frequency upshift of a factor 20–40, thus permitting to generate about 10^{10} – 10^9 fully coherent photons per shot in the tender x-ray range. These estimations exceed by one orders of magnitude the target values set by the MariX

scientific case, but do not take into account degradations due to errors, misalignment, jitters. MariX will be therefore capable to satisfy the requested FEL photon beam parameters expected by the envisaged experiments, considering also a safety margin dealing with the losses in delivering the photon beams to the experimental hutch. This source will permit the XAS/XMCD (with polarization control from quarterwavelength blades or undulators) and bulk photoemission applications and could become a highly efficient probe of matter at the nanoscale in bulk environments, as buried interfaces of interest in materials science, *in vivo* biological samples or catalysers at work. It will therefore create absolutely novel conditions for experiments that cannot be performed satisfactorily at the present and foreseen sources based on storage rings or SASE-FELs, and, due to its compact footprint, could be implemented in medium sized research laboratories and university campuses. The foreseen performances of MariX free electron laser are well beyond the state of the art of most of presently FELs in operation, and in the trailing edge of EuXFEL [51] and of the US future superconducting FEL project of reference, LCLS-II [52].

ORCID iDs

G Ghiringhelli  <https://orcid.org/0000-0003-0867-7748>

References

- [1] Rosenzweig J et al 2008 Generation of ultra-short, high brightness electron beams for single-spike SASE FEL operation *Nucl. Instrum. Methods Phys. Res. A* **593** 39
- [2] Marinelli A et al 2017 Experimental demonstration of a single-spike hard-x-ray free-electron laser starting from noise *Appl. Phys. Lett.* **111** 151101
- [3] Villa F et al 2017 Generation and characterization of ultra-short electron beams for single spike infrared FEL radiation at SPARC_LAB *Nucl. Instrum. Methods Phys. Res. A* **865** 43–6
- [4] Geloni G, Kocharyan V and Saldin E 2011 A novel self-seeding scheme for hard x-ray FELs *J. Mod. Opt.* **58** 1391–403
- [5] Amann J, Berg W et al 2012 Demonstration of self-seeding in a hard-x-ray free-electron laser *Nat. Photon.* **6** 693–8
- [6] ELETTRA light sources official webpage www.elettra.trieste.it/lightsources/index.html
- [7] Allaria E et al 2015 The FERMI free-electron lasers *J. Synchrotron Rad.* **22** 485–91
- [8] Giannessi L et al 2012 High-order-harmonic generation and superradiance in a seeded free-electron laser *Phys. Rev. Lett.* **108** 164801
- [9] Allaria E et al 2013 Two stage seeded soft-x-ray free-electron laser *Nat. Photon.* **7** 913–8
- [10] Yu L H et al 2000 High-gain harmonic-generation free-electron laser *Science* **289** 932
Doyuran A et al 2001 Characterization of a high-gain harmonic-generation free-electron laser at saturation *Phys. Rev. Lett.* **86** 5902
- [11] Yu L H et al 2003 First ultraviolet high-gain harmonic-generation free-electron laser *Phys. Rev. Lett.* **91** 074801
Togashi T et al 2011 Extreme ultraviolet free electron laser seeded with high-order harmonic of Ti:sapphire laser *Opt. Express* **19** 317
- [12] Giannessi L et al 2013 Superradiant cascade in a seeded free-electron laser *Phys. Rev. Lett.* **110** 044801
- [13] Takahashi E J et al 2004 Generation of strong optical field in soft x-ray region by using high-order harmonics *IEEE J. Sel. Top. Quantum Electron.* **10** 1315–28
- [14] Lambert G et al 2009 An optimized kHz two-colour high harmonic source for seeding free-electron lasers and plasma-based soft x-ray lasers *New J. Phys.* **11** 083033
- [15] Lambert G et al 2008 Injection of harmonics generated in gas in a free-electron laser providing intense and coherent extreme-ultraviolet light *Nat. Phys.* **4** 296
- [16] Labat M et al 2011 High-gain harmonic-generation free-electron laser seeded by harmonics generated in gas *Phys. Rev. Lett.* **107** 224801
- [17] Ackermann S et al 2013 Generation of coherent 19- and 38 nm radiation at a free-electron laser directly seeded at 38 nm *Phys. Rev. Lett.* **111** 114801
- [18] Xiang D and Stupakov G 2009 Echo-enabled harmonic generation free electron laser *Phys. Rev. Spec. Top. Accel. Beams* **12** 030702
- [19] Hemsing E et al 2016 Echo-enabled harmonics up to the 75th order from precisely tailored electron beams *Nat. Photon.* **10** 512
- [20] Feng C et al 2019 Coherent extreme ultraviolet free-electron laser with echo-enabled harmonic generation *Phys. Rev. Accel. Beams* **22** 050703
- [21] Ribič P R et al 2019 Coherent soft x-ray pulses from an echo-enabled harmonic generation free-electron laser nature research *Nat. Photon.* **13** 555
- [22] Ciocci F et al 1995 Design considerations on a high-power VUV FEL *IEEE J. Quantum Electron.* **31** 1242–52
- [23] McNeill B W J et al 2007 A design for the generation of temporally-coherent radiation pulses in the VUV and beyond by a self-seeded high gain free electron laser amplifier *New J. Phys.* **9** 239
- [24] Van der Slot P J M et al 2009 Time-dependent three dimensional simulation of free-electron laser oscillators *Phys. Rev. Lett.* **102** 244802
- [25] Kim K-J, Shvyd'ko Y and Reiche S 2008 A proposal for an x-ray oscillator with an energy recovery linac *Phys. Rev. Lett.* **100** 244802
- [26] Dattoli G, Di Palma E and Petralia A 2018 Free electron laser oscillator efficiency *Opt. Commun.* **425** 29
- [27] Marcus G et al 2019 Regenerative Amplification for a Hard-X Ray Free-Electron Laser *Proc. FEL TUP032*
- [28] Marcus G et al 2019 Cavity-Based Free-Electron Laser Research and Development: A Joint Argonne National Laboratory and SLAC National Laboratory Collaboration *Proc. FEL TUD04*
- [29] Huang Z and Ruth R D 2006 Fully coherent x-ray pulses from a regenerative-amplifier free-electron laser *Phys. Rev. Lett.* **96** 144801

- [30] Kim K-J and Shvyd'ko Y 2009 Tunable optical cavity for an x-ray free-electron laser oscillator *Phys. Rev. Spec. Top. Accel. Beams* **12** 030703
- [31] Li A K, Yan J, Feng C, Zhang M and Deng H 2018 High brightness fully coherent x-ray amplifier seeded by a free-electron laser oscillator *Phys. Rev. Accel. Beams* **21** 040702
- [32] Serafini L et al 2019 MariX, an advanced MHz-class repetition rate X-ray source for linear regime time-resolved spectroscopy and photon scattering *Nucl. Instrum. Methods Phys. Res. A* **930** 167–72
- [33] Bacci A et al 2019 Two-pass two-way acceleration in a super-conducting CW linac to drive low jitters x-ray FELs *Phys. Rev. Accel. Beams* **22** 111304
- [34] Vostroikov A, Sukhanov A, Yakovlev V and Solyak N 2015 Cumulative HOM excitation and transition effects in LCLS-II *Phys. Procedia* **79** 46–53
- [35] Hellert T, Ackermann W, Adolphsen C, De Gerssem H, Li Z and Mayes C 2018 Microphonic detuning induced coupler kick variation at LCLS-II *J. Phys. Conf. Ser.* **1067** 032015
- [36] Douglas D R et al 2006 Experimental investigations of multibunch, multipass beam breakup in the Jefferson laboratory free electron laser upgrade driver *Phys. Rev. Accel. Beams* **9** 064403
- [37] DESY XFEL Project Group 2007 *The European X-FEL Technical Design Report Paragraph 4.5.4 DESY 2006–097*
- [38] Petrillo V, Opromolla M, Bacci A, Drebot I, Ghiringhelli G, Petralia A et al 2019 High repetition rate and coherent free-electron laser in the x-rays range tailored for linear spectroscopy *Instruments* **3** 47
- [39] Di Mitri S and Cornacchia M 2015 Transverse emittance-preserving arc compressor for high brightness electron beam-based light sources and colliders *Europhys. Lett.* **109** 62002
- Di Mitri S 2016 Feasibility study of a periodic arc compressor in the presence of coherent synchrotron radiation *Nucl. Instrum. Methods Phys. Res. A* **806** 184
- [40] Placidi M et al 2017 Compact FEL-driven inverse Compton scattering gamma-ray source *Nucl. Instrum. Methods Phys. Res. A* **855** 55–60
- [41] Schröder S, Feigl T, Duparré A and Tünnermann A 2007 EUV reflectance and scattering of Mo/Si multilayers on differently polished substrates *Opt. Express* **15** 13997
- [42] Huang Q et al 2014 High efficiency structured EUV multilayer mirror for spectral filtering of long wavelengths *J. Opt. Soc. Am.* **22** 19365–19374
- [43] Zameshin A A, Yakshin A E, Chandrasekaran A and Bijkerk F 2019 Angular and spectral bandwidth of EUV multilayers near spacer material absorption edges *J. Nanosci. Nanotechnol.* **19** 602
- [44] Li K and Deng H 2018 Systematic design and three-dimensional simulation of x-ray FEL oscillator for Shanghai coherent light facility *Nucl. Instrum. Methods Phys. Res. A* **895** 40–7
- [45] Veronese M et al 2012 Intra Undulator Screen Diagnostics for the FERMI@Elettra FEL *Proc. of IBIC2012, TUPB76*
- [46] Capotondi F et al 2015 Multipurpose end-station for coherent diffraction imaging and scattering at FERMI@Elettra free-electron laser facility *J. Synchrotron Radiat.* **22** 544–52
- [47] Bodewadt J, RoBdach J and Hass E 2011 Commissioning Results of the Photon–Electron Diagnostic Unit at SFLASH *Proc. of DIPAC2011, MOPD54*
- [48] Belanger P A 1991 Beam propagation and the ABCD ray matrices *Opt. Lett.* **16** 196
- [49] Ben-Zvi I, Yung K M and Yu L-H 1992 The ‘fresh-bunch’ technique in FELs *Nucl. Instrum. Methods Phys. Res. A* **318** 726
- [50] Reiche S 1999 GENESIS 1.3: a fully 3D time-dependent FEL simulation code *Nucl. Instrum. Methods Phys. Res. A* **429** 243
- [51] Weise H and Decking W 2017 Commissioning and First Lasing of the European XFEL FEL2017, *Int. Free Electron Laser Conf., MOC03*
- [52] Raubenheimer T 2016 LCLS-II-HE FEL Facility overview [www//portal.slac.stanford.edu/sites/conf_public/lclsiie2016/Documents/160926%20LCLS-II-HE%20Raubenheimer.pdf](http://portal.slac.stanford.edu/sites/conf_public/lclsiie2016/Documents/160926%20LCLS-II-HE%20Raubenheimer.pdf).